Disentangling the impact of the COVID-19 lockdowns on urban NO2 from natural variability

Daniel L. Goldberg[1], Susan C Anenberg[1], Debora Griffin[2], Chris A Mclinden[2], Zifeng Lu[3], and David G Streets[3]

[1]George Washington University
[2]Environment and Climate Change Canada
[3]Argonne National Laboratory

November 22, 2022

Abstract

Satellite data show substantial drops in nitrogen dioxide (NO2) during COVID-19 physical distancing. To attribute NO2 changes to NOx emissions changes over short timescales, one must account for meteorological effects. We find that meteorological patterns were especially favorable for low NO2 in much of the U.S. in spring 2020, complicating comparisons with spring 2019. Meteorological variations between years can cause column NO2 differences of ˜15% over monthly timescales. After accounting for sun angle and meteorological considerations, we calculate that NO2 drops ranged between 9.2 – 43.4% among twenty cities in North America, with a median of 21.6%. Of the studied cities, largest NO2 drops (>30%) were in San Jose, Los Angeles, and Toronto, and smallest drops (<12%) were in Miami, Minneapolis, and Dallas. These normalized NO2 changes can be used to highlight locations with greater activity changes and better understand the sources contributing to adverse air quality in each city.

Disentangling the impact of the COVID-19 lockdowns on urban NO_2 from natural variability

Daniel L. Goldberg*[,1,3], Susan C. Anenberg[1], Debora Griffin[2], Chris A. McLinden[2], Zifeng Lu[3], David G. Streets[3]

[1]Department of Environmental and Occupational Health, George Washington University, Washington, DC, U.S.

[2]Air Quality Research Division, Environment and Climate Change Canada (ECCC), Toronto, Ontario, Canada

[3]Energy Systems Division, Argonne National Laboratory, Lemont, IL, U.S.

[*]Corresponding author. Phone: (202)994-8102; Email: dgoldberg@gwu.edu

Abstract

Satellite data show substantial drops in nitrogen dioxide (NO_2) during COVID-19 physical distancing. To attribute NO_2 changes to NO_X emissions changes over short timescales, one must account for meteorological effects. We find that meteorological patterns were especially favorable for low NO_2 in much of the U.S. in spring 2020, complicating comparisons with spring 2019. Meteorological variations between years can cause column NO_2 differences of ~15% over monthly timescales. After accounting for sun angle and meteorological considerations, we calculate that NO_2 drops ranged between 9.2 – 43.4% among twenty cities in North America, with a median of 21.6%. Of the studied cities, largest NO_2 drops (>30%) were in San Jose, Los Angeles, and Toronto, and smallest drops (<12%) were in Miami, Minneapolis, and Dallas. These normalized NO_2 changes can be used to highlight locations with greater activity changes and better understand the sources contributing to adverse air quality in each city.

Plain-Language Summary

The current paradigm of disentangling emissions from meteorological influences on air pollution by averaging over many months has insufficient temporal granularity to quantify short-term emission changes. We developed two novel methods to account for weather impacts on daily pollution levels during COVID-19 precautions. Once we accounted for favorable weather conditions that in some cases kept air pollution low independent of tail-pipe emissions, calculated air pollutant emission reductions varied dramatically (9 – 43%) among twenty North American cities. Results can be used to understand factors contributing to inconsistent NO_2 changes during physical distancing, which can inform the effectiveness of COVID-19 protocols and aid future policy development. These methodologies will allow us to respond more quickly in future unintended experiments when emissions change suddenly.

1. Introduction

Nitrogen dioxide (NO_2) is unique due to its relatively short photochemical lifetime which varies from 2-6 h during the summer daytime (Beirle et al., 2011; de Foy et al., 2014; Laughner & Cohen, 2019; Valin et al., 2013) to 12-24 h during winter (Beirle et al., 2003; Shah et al., 2020). As a result, tropospheric NO_2 concentrations are strongly correlated with local NO_X emissions, which are often anthropogenic in origin. However, due to the effects of meteorology and sun angle on the NO_2 abundance, NO_2 can vary by a factor of two simply due to seasonal changes (Pope et al., 2015; Wang et al., 2019). Therefore, satellite data are typically averaged over long timeframes (~seasonal/annual) to assess changes in NO_X emissions (Duncan et al., 2016; Geddes et al., 2016; Georgoulias et al., 2019; Hilboll et al., 2013, 2017; Kim et al., 2009; Krotkov et al., 2016; Lamsal et al., 2015; McLinden et al., 2016; VanDerA et al., 2008).

With the COVID-19 crisis, there is now broad interest in rapid assessments of NOx emission changes on short timescales in locations that have implemented stay-at-home orders or other physical distancing measures. Using satellite data in this instance can be advantageous due to its global coverage at immediate timescales. However, current methods of averaging satellite NO_2 data over many months to minimize random daily effects of weather will not provide the temporal granularity needed to quantify short-lived NO_X emission changes.

Preliminary satellite-based studies indicate that NO_2 dropped substantially in China following stringent COVID-19 physical distancing actions (F. Liu et al., 2020; Zhang et al., 2020). Similar declines have also been seen over northern Italy (ESA, 2020b) and India (ESA, 2020a). Although lockdown measures – and adherence to them – have been looser in the U.S. than in China, India, and Italy, preliminary analyses show that NO_2 amounts are declining across U.S. cities as well (NASA, 2020). These declines have, in some cases in the media (Holcombe & O'Key, 2020; Plumer & Popovich, 2020), been attributed to the emission changes during lockdowns, without accounting for the potentially substantial influences of meteorology and seasonality. Accounting for natural NO_2 fluctuations are especially important during spring, a time when the NO_2 concentrations and lifetimes are quickly changing due to transitioning meteorology, sun angle, and snow cover.

Understanding how NOx emissions have changed in response to physical distancing measures requires new methods to account for sun angle and meteorological conditions over very short time scales (days/weeks), as opposed to the traditional method of averaging over seasons and years. Here, we use three different methods to assess the NO_2 decreases associated with COVID-19 lockdowns. We combine TROPOMI NO_2 data with ERA5 re-analysis and a regional chemical transport model to determine the effects of the sun angle and meteorological factors – such as wind speed and wind direction – on NO_2 column amounts. The NO_2 changes after this "normalization" are more likely to represent the NOx emissions changes due to COVID-19.

2. Methods

2.1 TROPOMI NO_2

TROPOMI was launched by the European Space Agency (ESA) for the European Union's Copernicus Sentinel 5 Precursor (S5p) satellite mission on October 13, 2017. The satellite follows a sun-synchronous, low-earth (825 km) orbit with a daily equator overpass time of approximately 13:30 local solar time (VanGeffen et al., 2019). TROPOMI measures total column amounts of several trace gases in the Ultraviolet-Visible-Near Infrared-Shortwave Infrared spectral regions (Veefkind et al., 2012). At nadir, pixel sizes are 3.5×7 km^2 (reduced to 3.5×5.6 km^2 on August 6, 2019) with little variation in pixel sizes across the 2600 km swath.

Using a differential optical absorption spectroscopy (DOAS) technique on the radiance measurements in the 405 – 465 nm spectral window, the top-of-atmosphere spectral radiances can be converted into slant column amounts of NO_2 between the sensor and the Earth's surface (Boersma et al., 2018). In two additional steps, the slant column quantity can be converted into a tropospheric vertical column content, which is the quantity used most often to further our understanding of NO_2 in the atmosphere (Beirle et al., 2019; Dix et al., 2020; Goldberg et al., 2019; Griffin et al., 2019; Ialongo et al., 2020; Reuter et al., 2019; Zhao et al., 2020).

2.2 Meteorological Dataset

We use ERA5 meteorology((C3S), 2017) for the wind speed and direction in our analysis. When filtering the data based on wind, we use the average 100-m winds during 16 – 21 UTC, which approximately corresponds to the TROPOMI overpass time over North America. To downscale the ERA5 re-analysis, which is provided at $0.25° \times 0.25°$, we spatially interpolate daily averaged winds to $0.01° \times 0.01°$ using bilinear interpolation. Due to our dependence on $0.25° \times 0.25°$

meteorology, any microscale features (e.g., sea breezes) will not be accounted for, but these effects should be minor for our particular analysis.

2.3 Calculation of NO_2 Changes

We calculate the NO_2 changes using three different methods. In Method 1, we compare an average of March 15, 2020 – April 30, 2020 to the same timeframe of 2019; this year-over-year comparison is used most often in satellite studies quantifying long-term changes in NO_X emissions. In Method 2, we develop a strategy to account for varying weather patterns without the use of a chemical transport model. In this method, we normalize each day's NO_2 observation to a day with "standard" meteorology – similar to standard temperature and pressure (STP) conditions in a laboratory setting. We do this by accounting for four different day-varying effects; these are sun angle, wind speed, wind direction, and day-of-week. In all cases, we normalize city-specific conditions to those that are climatological on April 15th. Finally, in Method 3, we infer a TROPOMI NO_2 column amount under normal circumstances using the GEM-MACH regional chemical transport model, and then compare the actual TROPOMI columns to the theoretical columns. Methods 2 & 3, both account for year-varying meteorology, while Methods 1 does not. A detailed description of Methods 2 & 3 can be found in the Supplemental.

3. Results

3.1 Sun Angle & Meteorological Relationships

In the top row of Figure 1, we show 2019 NO_2 column densities during the low sun-angle “cold” season (January – March, October – December) and high sun-angle “warm” season (May – September) in the continental United States and southern Canada.

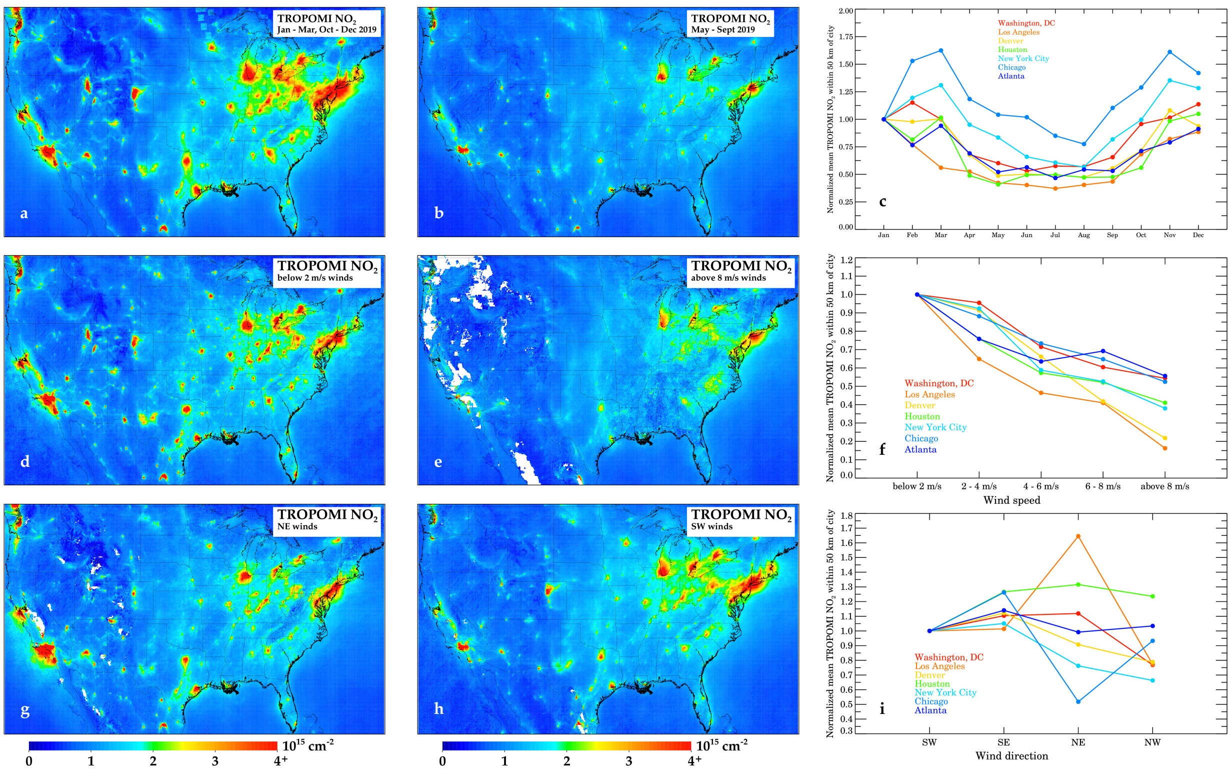

Figure 1. Effects of meteorology and sun angle on column NO_2. Top panels show (a) TROPOMI NO_2 during the warm season (May – Sept 2019), (b) during the cold season (Jan – Mar, Oct – Dec 2019), and (c) the monthly variation in 7 U.S. cities normalized to Jan 2019. Middle panels show (d) TROPOMI NO_2 when winds are < 2 m/s, (e) when winds are > 8 m/s, and (f) variations in NO_2 as a function of wind speed for seven cities normalized to stagnant conditions. Bottom panels show (g) TROPOMI NO_2 when winds are southwesterly, (h) when winds are northeasterly, and (i) variations as a function of wind direction for seven cities normalized to southwesterly winds.

Column NO_2 is larger during the cold season than during the warm season over the majority of our domain, despite NO_X emissions generally peaking during the middle of the warm season due to a heavy air conditioning load (Abel et al., 2017; He et al., 2013). The larger NO_2 concentrations during the winter are instead due to the longer NO_2 lifetime during the cold season, primarily due to slower photolysis rates. When NO_X is emitted during the warm season, it is transformed into other chemical species, such as O_3 and HNO_3, more quickly than during the winter. We find that in most near-urban locations column NO_2 amounts are 1.5 – 3 times larger during the winter than during the summer, and can vary substantially between city.

In a next step, we account for wind speed and wind direction in the spatiotemporal variation of NO_2 columns. In the middle and bottom panels of Figure 1, we demonstrate the effects of wind speed and wind direction on the NO_2 in our domain. Increases in wind speed yield NO_2 decreases due to quicker dispersion away from the city centers. For example, in New York City, Washington DC, Atlanta, and Chicago, all cities with relatively flat topography and located in the eastern United States, increasing wind speeds from nearly stagnant to > 8 m/s decreases NO_2 by 30 – 60%. Conversely, in Denver and Los Angeles, cities with more heterogeneous topography and with general isolation from an agglomeration of cities, show a stronger dependence on wind speed; increasing wind speeds from nearly stagnant to > 8 m/s decreases NO_2 by 70 – 85%. In both instances, these examples show the strong dependence of wind speed on local NO_2 amounts.

Similarly, wind direction has a large role in the local NO_2 amounts, although the effects of wind direction are non-linear. Generally, northwest winds yield the cleanest conditions in most U.S. cities, but the effects of other wind directions are more nuanced. For example, southwesterly winds yield the worst air quality in New York City, while northeasterly winds yield the largest NO_2 in Washington, D.C. This is due to the fact that the other city lies upwind in each opposing scenario. Changes in wind direction, given the same wind speed, can yield differences in NO_2 in major cities by up to 70%, and must be accounted for if properly attributing NO_2 changes to NO_X emissions. Climatological patterns for all cities are shown in the Supplemental Material (Figures S1-S3).

While 2-m air temperature and boundary layer depth may be affecting the NO_2 concentrations, these are not independent of the aforementioned factors: sun angle, wind speed and wind direction. In fact, sun angle, wind speed, and wind direction are by themselves highly skilled predictors of near-surface temperatures and boundary layer depth in most instances. Since we are focused on mostly clear-sky days, clouds have limited effects here. Previous day's precipitation may also be a contributing factor to daily NO_2 amounts, but in many areas, the wind direction will partially account for this, since northwest winds usually follow large rain events in most areas.

3.2 Effects of COVID-19 physical distancing on NO_2

In order to quantify rapid changes in NO_X due to COVID-19 physical distancing, we calculate NO_2 changes in North American cities using three different methods and a reference method. The results for all cities are shown in Table 1.

Table 1. Percentage drop in column NO_2 as observed by TROPOMI. Cities are listed by largest to smallest reduction as determined by the median of all three methods.

	Reference case	**Account for sun-angle only**	**Account for sun-angle & meteorology**			
	Method 0	**Method 1**	**Method 2**	**Method 3**		
City Name	**Δ between months 2020 only (Jan-Feb vs. Mar 15 - Apr 30)**	**Δ between years 2019 vs. 2020 (Mar 15 - Apr 30)**	**Using ERA5 analogs to account for meteorology 2019 vs. 2020 (Mar 15 - Apr 30)**	**Using GEM-MACH to infer NO2, 2020 only (Mar 15 - Apr 30)**	***Mean of Methods 1-3***	***Median of Methods 1-3***
San Jose	65.2%	43.4%	40.7%	43.5%	42.5%	**43.4%**
Los Angeles	66.1%	32.6%	32.5%	38.6%	34.6%	**32.6%**
Toronto	60.4%	31.0%	17.0%	42.0%	30.0%	**31.0%**
Philadelphia	50.3%	36.6%	30.7%	22.1%	29.8%	**30.7%**
Denver	25.8%	29.2%	23.4%	39.1%	30.6%	**29.2%**
Atlanta	39.6%	35.2%	27.4%	20.2%	27.6%	**27.4%**
Detroit	35.5%	29.9%	22.8%	15.6%	22.8%	**22.8%**
Boston	40.3%	22.8%	23.5%	17.8%	21.4%	**22.8%**
Washington DC	42.9%	31.4%	21.2%	6.7%	19.8%	**21.2%**
Montreal	12.5%	3.3%	20.9%	30.2%	18.1%	**20.9%**
New York City	32.7%	20.2%	20.0%	17.9%	19.4%	**20.0%**
New Orleans	41.7%	13.5%	19.6%	22.5%	18.5%	**19.6%**
Las Vegas	66.7%	9.5%	18.4%	42.0%	23.3%	**18.4%**
Houston	38.9%	26.3%	15.6%	1.9%	14.6%	**15.6%**
Chicago	31.0%	23.6%	14.9%	3.5%	14.0%	**14.9%**
Phoenix	43.9%	12.8%	14.8%	35.4%	21.0%	**14.8%**
Austin	34.3%	14.5%	9.4%	16.1%	13.3%	**14.5%**
Dallas	41.9%	11.9%	3.6%	16.7%	10.7%	**11.9%**
Miami	27.9%	16.1%	-1.6%	11.0%	8.5%	**11.0%**
Minneapolis	0.1%	14.3%	9.2%	8.1%	10.5%	**9.2%**
Mean of each method	39.9%	22.9%	19.2%	22.5%	21.6%	**21.6%**

The reference method, Method 0, compares the pre-lockdown and post-lockdown periods and represents the "true" NO_2 change; however, this method does not account for seasonal changes and, thus, is not considered in the medians/means.

In Method 1, we compare an average of March 15, 2020 – April 30, 2020 to the same timeframe of 2019. In Figure 2, we show difference and ratio plots between these two years (i.e., Method

1). The largest decreases in NO_2 are near the major cities in North America. We also find regional decreases in the eastern North America. Conversely, the central and northwestern United States have seen little change between years, which is likely due to the high fraction of NO_2 attributed to biogenic sources and long-range transport. We also observe substantial decreases near retired electricity generating units in the western U.S. (Storrow, 2019)

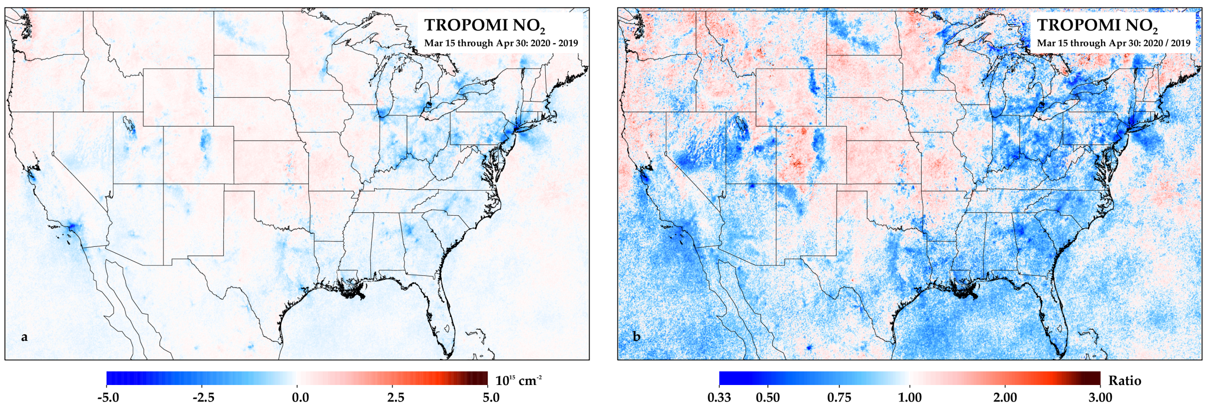

Figure 2. TROPOMI NO_2 differences between 2019 & 2020, using March 15 – April 30, 2020 as the post-COVID-19 period. Plots are showing (a) the absolute difference and (b) the ratio between years.

In Figure 3, we demonstrate Method 2. Here, we show the 2019 and 2020 28-day running TROPOMI NO_2 medians after accounting for sun angle and meteorology. In this figure, the January values are uniformly lower than their true values (Figure S4) because we are normalizing to April meteorological conditions (i.e., sun angle is higher in April as compared to January). In New York City, we calculate a 20.0% drop in NO_2 due to COVID-19 precautions. We find that there is no difference between Method 2 – which accounts for meteorology – and Method 1 – which only accounts for sun angle. This suggests that varying meteorological conditions in New York City, while different between years, may not have had a strong biasing effect. However, in Washington D.C. we find favorable conditions in 2020 as compared to 2019 because we observe substantially different NO_2 drops before (31.4%) and after (21.2%) correcting for the meteorology. These results are corroborated by the wind speed and direction (Figure S5). In 2019, winds were on average southwesterly, while in 2020, winds had more of a northwesterly and therefore cleaner component. Of all cities analyzed, we find that Miami had the most favorable conditions for low NO_2 in 2020 as compared to 2019; in 2020, winds were stronger from the south – in this case a cleaner air mass – than in 2019, which had relatively stagnant winds. Conversely, in Montreal, New Orleans, and Las Vegas, meteorological conditions appeared to be unfavorable in 2020 as compared to 2019.

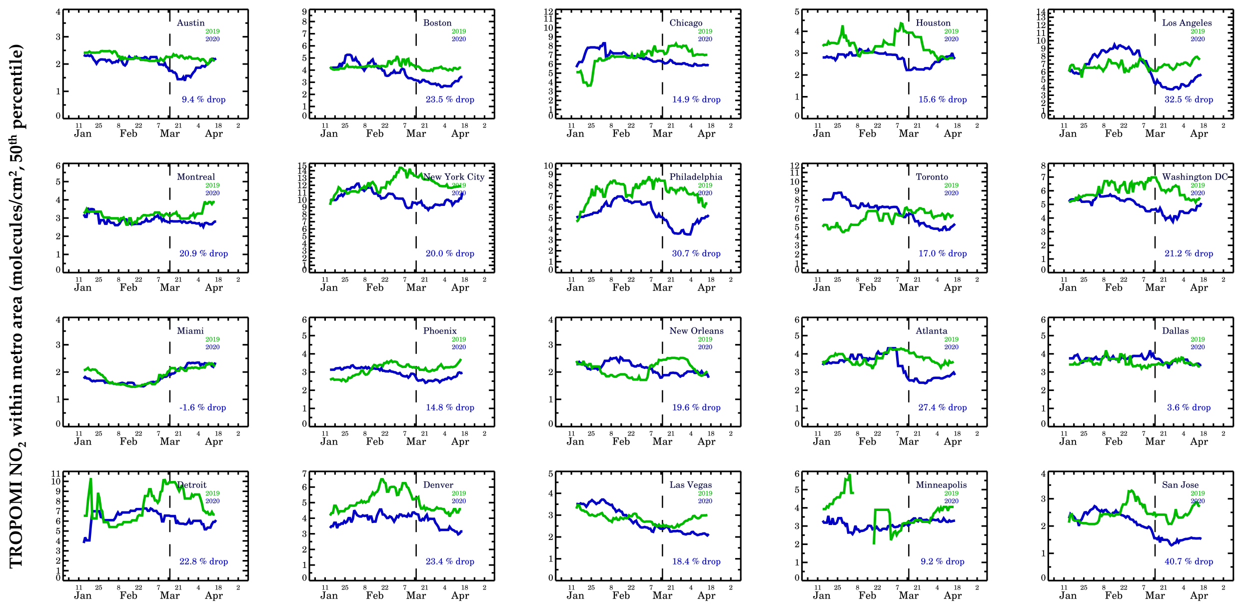

Time series (28-day rolling medians after normalizing for sun angle and meteorology)

Figure 3. Trends in TROPOMI NO_2 since January 1 in 2019 and 2020 after accounting for meteorological variability and sun angle. The lines represent the 28-day rolling median value (50th percentile) in a 0.4° × 0.4° box centered on the city center for the largest cities (New York City, Los Angeles, Chicago, Toronto, Houston) and 0.2° × 0.2° box in all other cities.

In Figure 4, we demonstrate Method 3, in which we account for meteorology and chemical interactions using a chemical transport model. We create a theoretical TROPOMI column NO_2 using ECCC's regional operational air quality forecast model (Moran et al., 2009; Pendlebury et al., 2018), which accounts for typical seasonal emission changes but not for any impacts due to the COVID-19 lockdowns; this helps provide expected NO_2 levels with a business as usual scenario. Around mid-March there is often a divergence between the expected and observed NO_2 in the major cities. Using this method, largest NO_2 reductions due to COVID-19 precautions are in Toronto, San Jose, and Las Vegas. Similar to Method 2, we find that NO_2 changes are generally smaller in the Northeastern U.S. and Florida as compared to Method 1 after accounting for meteorology. In fifteen of the twenty studied cities, we find that Methods 2 & 3, which utilize independent meteorological datasets, show similar biasing effects of meteorology (favorable vs. unfavorable) when compared to Method 1.

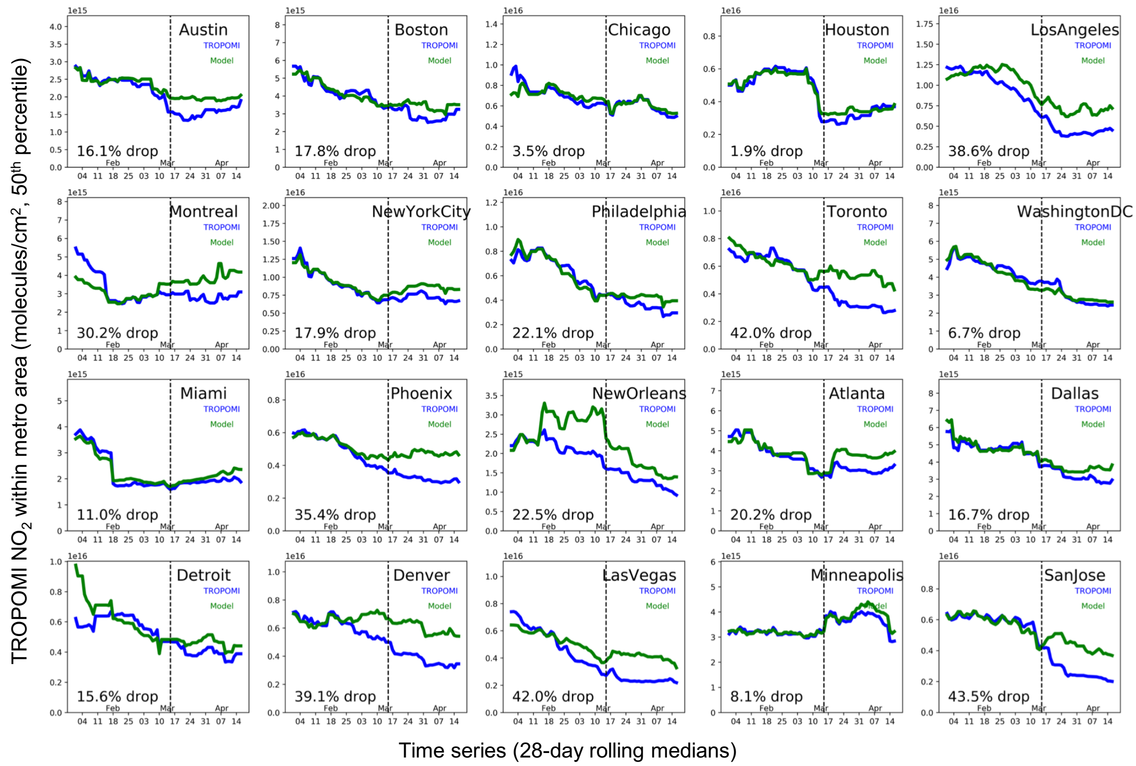

Figure 4. Trends in TROPOMI NO_2 since January 1, 2020. The actual observed columns are shown in black, while the "expected" columns - using GEM-MACH to infer NO_2 in the absence of lockdowns – is shown in blue. The lines represent the 28-day rolling median value (50th percentile) in a 0.4° × 0.4° box centered on the city center for the largest cities (New York City, Los Angeles, Chicago, Toronto, Houston) and 0.2° × 0.2° box in all other cities.

4. Discussion

Here we demonstrate two methodologies, Methods 2 & 3, to account for time-varying effects of meteorology on NO_2 concentrations. There are two main advantages for using Methods 2 & 3 to assess rapid changes in NO_X as compared to a year-to-year comparison of the same month or seasonal period. Year-over-year technological improvements in the United States are generally causing NO_X emissions to decrease over time, although we find a statistically insignificant NO_2 increase of 0.6% in our cities between 2019 and 2020 in the January – February average. Accounting for year-over-year changes would be more important if comparing 2020 values to years preceding 2019.

Perhaps more importantly, there are often different seasonal patterns between years, even when averaged over the entire season. Many longer-term meteorological patterns in North America can be attributed to the El Nino South Oscillation (ENSO) or the North Atlantic Oscillation

(NAO). In particular relevance to this analysis, the January – March 2019 period had a persistently negative NAO (https://www.cpc.ncep.noaa.gov/products/precip/CWlink/pna/month_nao_index.shtml) which allowed Arctic air to more readily intrude into the northern US than during more typical winters (https://www.ncdc.noaa.gov/sotc/national/201902). In January – March 2020, there was a consistently positive NAO which limited the influence of cold and relatively clean Arctic air in eastern North America, but instead yielded cloudier and wetter conditions. Similarly, ENSO can affect air quality in cities (Edwards et al., 2019; Shen & Mickley, 2017), but this had a minor effect between 2019 (Oceanic Niño Index: +0.8) and 2020 (Oceanic Niño Index: +0.5).

5. **Conclusions**

We estimate that NO_X emissions temporarily dropped between 9 – 43% in North American cities due to COVID-19 precautions, with a median drop of 21.6% before and after COVID-19 physical distancing. If the sun angle is not accounted for, then the median NO_2 drop is 39.9%; this represents the true change of NO_2 in cities, but is not analogous to a change in NO_X emissions. Our reported median drop of 21.6% is marginally lower than the 22.9% in a simple year-to-year comparison, which suggests that 2020 meteorology was slightly favorable for lower NO_2, although these effects are most pronounced in the Northeastern United States and Florida.

A deficiency of our method is our reliance on a single satellite instrument and algorithm. It is known that the operational TROPOMI NO_2 algorithm underestimates tropospheric vertical column NO_2 in urban areas due to its reliance on a global model to provide shape profiles for the air mass factor (AMF); investigating the effects of the AMF bias on trends will be the subject of future work. Also, there may be a clear-sky bias (Geddes et al., 2012) associated with TROPOMI retrievals, but the results presented here are generally consistent with studies using ground monitors over the coincident region (Bekbulat et al., 2020) and the reported CO_2 emissions reductions due to COVID-19 precautions (Le Quéré et al., 2020).

The estimates of NO_2 changes using our Methods appear to be reasonable given a quick bottom-up emissions calculation. Assuming that passenger vehicles traffic dropped by ~50%, and that all other sources only dropped modestly ~10 – 25%, NO_X reductions between 10 – 35% would be expected. San Jose, Los Angeles and Toronto appear to have reductions at the high end of this range, while Miami, Minneapolis, and Dallas have values near the lowest end; further work will look into why these cities have reductions on the ends of the spectrum. Rapid assessments of NO_2 changes – after normalized for seasonal and meteorological factors – can be used to highlight locations with greater changes in activity and better understand the sources contributing to adverse air quality in each city.

Acknowledgments

This work has been supported by NASA through a Rapid Response grant, a Health and Air Quality (HAQ) grant (award #: 80NSSC19K0193), and two Atmospheric Composition Modeling and Analysis Program grants. The work has also been supported by the Department of Energy, Office of Fossil Energy. We would also like to acknowledge valuable comments during the manuscript preparation from Joanna Joiner and Lok Lamsal of NASA Goddard, Joel Dreessen of Maryland Department of the Environment, Lucas Henneman of Harvard University T.H. Chan School of Public Health, and A.R. "Ravi" Ravishankara of Colorado State University. TROPOMI NO_2 data can be freely downloaded from the European Space Agency Copernicus Open Access Hub or the NASA EarthData Portal (http://doi.org/10.5270/S5P-s4ljg54). ERA5 can be freely downloaded from the Copernicus Climate Change (C3S) climate data store (CDS) (https://cds.climate.copernicus.eu/#!/search?text=ERA5&type=dataset). The submitted manuscript has been created by UChicago Argonne, LLC, Operator of Argonne National Laboratory ("Argonne"). Argonne, a US Department of Energy Office of Science laboratory, is operated under contract no. DE-AC02-06CH11357.

Author Contributions

DLG drafted the concept, wrote the manuscript, and performed much of the analysis. SCA jointly drafted the concept and edited the manuscript. DG and CAM provided the regional chemical model data and related analysis, and edited the manuscript. ZL jointly drafted the concept, helped to process the TROPOMI NO_2 data, and edited the manuscript. DGS edited the manuscript.

References

(C3S), C. C. C. S. (2017). ERA5: Fifth generation of ECMWF atmospheric reanalyses of the global climate. Retrieved May 1, 2020, from https://cds.climate.copernicus.eu/cdsapp#!/home

Abel, D. W., Holloway, T., Kladar, R. M., Meier, P., Ahl, D., Harkey, M., & Patz, J. (2017). Response of Power Plant Emissions to Ambient Temperature in the Eastern United States. *Environmental Science and Technology*, *51*(10), 5838–5846. https://doi.org/10.1021/acs.est.6b06201

Beirle, S., Platt, U., Wenig, M., & Wagner, T. (2003). Weekly cycle of NO2 by GOME measurements: A signature of anthropogenic sources. *Atmospheric Chemistry and Physics*, *3*(6), 2225–2232. https://doi.org/10.5194/acp-3-2225-2003

Beirle, S., Boersma, K. F., Platt, U., Lawrence, M. G., & Wagner, T. (2011). Megacity Emissions and Lifetimes of Nitrogen Oxides Probed from Space. *Science*, *333*(6050), 1737–1739. https://doi.org/10.1126/science.1207824

Beirle, S., Borger, C., Dörner, S., Li, A., Hu, Z., Liu, F., et al. (2019). Pinpointing nitrogen oxide emissions from space. *Science Advances*, *5*(11), eaax9800. https://doi.org/10.1126/sciadv.aax9800

Bekbulat, B., Apte, J. S., Millet, D. B., Robinson, A. L., Wells, K., & Marshall, J. D. (2020). PM 2.5 and ozone air pollution levels have not dropped consistently across the US followingsocietal covid response. https://doi.org/10.26434/CHEMRXIV.12275603

Boersma, K. F., Eskes, H. J., Richter, A., De Smedt, I., Lorente, A., Beirle, S., et al. (2018). Improving algorithms and uncertainty estimates for satellite NO2 retrievals: results from the quality assurance for the essential climate variables (QA4ECV) project. *Atmospheric Measurement Techniques*, *11*(12), 6651–6678. https://doi.org/10.5194/amt-11-6651-2018

Choi, S., Lamsal, L. N., Follette-Cook, M., Joiner, J., Krotkov, N. A., Swartz, W. H., et al. (2019). Assessment of NO2 observations during DISCOVER-AQ and KORUS-AQ field campaigns. *AMTD*. https://doi.org/10.5194/amt-2019-338

Dix, B., Bruin, J., Roosenbrand, E., Vlemmix, T., Francoeur, C., Gorchov-Negron, A., et al. (2020). Nitrogen Oxide Emissions from U.S. Oil and Gas Production: Recent Trends and Source Attribution. *Geophysical Research Letters*, *47*(1), 2019GL085866. https://doi.org/10.1029/2019GL085866

Duncan, B. N., Lamsal, L. N., Thompson, A. M., Yoshida, Y., Lu, Z., Streets, D. G., et al. (2016). A space-based, high-resolution view of notable changes in urban NOx pollution around the world (2005-2014). *Journal of Geophysical Research: Atmospheres*, *121*(2), 976–996. https://doi.org/10.1002/2015JD024121

Edwards, R. P., Engle, M., & Morris, G. (2019). Evaluation of El Niño-Southern oscillation influence on ozone exceedances along the United States Gulf Coast. *Atmospheric Environment*, 117127. https://doi.org/10.1016/j.atmosenv.2019.117127

ESA. (2020a). Air pollution drops in India following lockdown. Retrieved May 4, 2020, from http://www.esa.int/Applications/Observing_the_Earth/Copernicus/Sentinel-5P/Air_pollution_drops_in_India_following_lockdown

ESA. (2020b). Coronavirus: nitrogen dioxide emissions drop over Italy. Retrieved May 4, 2020, from http://www.esa.int/ESA_Multimedia/Videos/2020/03/Coronavirus_nitrogen_dioxide_emissions_drop_over_Italy

de Foy, B., Wilkins, J. L., Lu, Z., Streets, D. G., & Duncan, B. N. (2014). Model evaluation of methods for estimating surface emissions and chemical lifetimes from satellite data. *Atmospheric Environment*, *98*, 66–77. https://doi.org/10.1016/j.atmosenv.2014.08.051

Geddes, J. A., Murphy, J. G., O'Brien, J. M., & Celarier, E. A. (2012). Biases in long-term NO2 averages inferred from satellite observations due to cloud selection criteria. *Remote Sensing of Environment*, *124*(2), 210–216. https://doi.org/10.1016/j.rse.2012.05.008

Geddes, J. A., Martin, R. V., Boys, B. L., & van Donkelaar, A. (2016). Long-Term Trends Worldwide in Ambient NO 2 Concentrations Inferred from Satellite Observations. *Environmental Health Perspectives*, *124*(3), 281–289. https://doi.org/10.1289/ehp.1409567

van Geffen, J., Boersma, K. F., Eskes, H., Sneep, M., ter Linden, M., Zara, M., & Veefkind, J. P. (2020). S5P TROPOMI NO₂ slant column retrieval: method, stability, uncertainties and comparisons with OMI. *Atmospheric Measurement Techniques*, *13*(3), 1315–1335. https://doi.org/10.5194/amt-13-1315-2020

Georgoulias, A. K., van der A, R. J., Stammes, P., Boersma, K. F., & Eskes, H. J. (2019). Trends and trend reversal detection in 2 decades of tropospheric NO2 satellite observations. *Atmospheric Chemistry and Physics*, *19*(9), 6269–6294. https://doi.org/10.5194/acp-19-6269-2019

Goldberg, D. L., Lamsal, L. N., Loughner, C. P., Swartz, W. H., Lu, Z., & Streets, D. G. (2017). A high-resolution and observationally constrained OMI NO2 satellite retrieval. *Atmospheric Chemistry and Physics*, *17*(18), 11403–11421. https://doi.org/10.5194/acp-17-11403-2017

Goldberg, D. L., Lu, Z., Streets, D. G., de Foy, B., Griffin, D., McLinden, C. A., et al. (2019). Enhanced Capabilities of TROPOMI NO2 : Estimating NOx from North American Cities and Power Plants. *Environmental Science & Technology*, acs.est.9b04488. https://doi.org/10.1021/acs.est.9b04488

Griffin, D., Zhao, X., McLinden, C. A., Boersma, K. F., Bourassa, A., Dammers, E., et al. (2019). High-Resolution Mapping of Nitrogen Dioxide With TROPOMI: First Results and Validation Over the Canadian Oil Sands. *Geophysical Research Letters*, *46*(2), 1049–1060. https://doi.org/10.1029/2018GL081095

He, H., Hembeck, L., Hosley, K. M., Canty, T. P., Salawitch, R. J., & Dickerson, R. R. (2013). High ozone concentrations on hot days: The role of electric power demand and NOx emissions. *Geophysical Research Letters*, *40*(19), 5291–5294. https://doi.org/10.1002/grl.50967

Hilboll, A., Richter, A., & Burrows, J. P. (2013). Long-term changes of tropospheric NO2 over megacities derived from multiple satellite instruments. *Atmospheric Chemistry and Physics*, *13*(8), 4145–4169. https://doi.org/10.5194/acp-13-4145-2013

Hilboll, A., Richter, A., & Burrows, J. P. (2017). NO2 pollution over India observed from space - the impact of rapid economic growth, and a recent decline. *Atmospheric Chemistry and Physics Discussions*, *20*(2), 1–18. https://doi.org/10.5194/acp-2017-101

Holcombe, M., & O'Key, S. (2020). Satellite images show less pollution over the US as coronavirus shuts down public places. Retrieved from https://www.cnn.com/2020/03/23/health/us-pollution-satellite-coronavirus-scn-trnd/index.html

Ialongo, I., Virta, H., Eskes, H., Hovila, J., & Douros, J. (2020). Comparison of TROPOMI/Sentinel-5 Precursor NO2 observations with ground-based measurements in Helsinki. *Atmospheric Measurement Techniques*, *13*(1), 205–218. https://doi.org/10.5194/amt-13-205-2020

Kim, S. W., Heckel, A., Frost, G. J., Richter, A., Gleason, J., Burrows, J. P., et al. (2009). NO2 columns in the western United States observed from space and simulated by a regional chemistry model and their implications for NOx emissions. *Journal of Geophysical Research Atmospheres*, *114*(11), 1–29. https://doi.org/10.1029/2008JD011343

Kleipool, Q. L., Dobber, M. R., de Haan, J. F., & Levelt, P. F. (2008). Earth surface reflectance climatology from 3 years of OMI data. *Journal of Geophysical Research Atmospheres*, *113*(18), 1–22. https://doi.org/10.1029/2008JD010290

Krotkov, N. A., McLinden, C. A., Li, C., Lamsal, L. N., Celarier, E. A., Marchenko, S. V., et al. (2016). Aura OMI observations of regional SO2 and NO2 pollution changes from 2005 to 2015. *Atmospheric Chemistry and Physics*, *16*(7), 4605–4629. https://doi.org/10.5194/acp-16-4605-2016

Lamsal, L. N., Krotkov, N. A., Celarier, E. A., Swartz, W. H., Pickering, K. E., Bucsela, E. J., et al. (2014). Evaluation of OMI operational standard NO2 column retrievals using in situ and surface-based NO2 observations. *Atmospheric Chemistry and Physics*, *14*(21), 11587–11609. https://doi.org/10.5194/acp-14-11587-2014

Lamsal, L. N., Duncan, B. N., Yoshida, Y., Krotkov, N. A., Pickering, K. E., Streets, D. G., & Lu, Z. (2015). U.S. NO2 trends (2005-2013): EPA Air Quality System (AQS) data versus improved observations from the Ozone Monitoring Instrument (OMI). *Atmospheric Environment*, *110*(2), 130–143. https://doi.org/10.1016/j.atmosenv.2015.03.055

Laughner, J. L., & Cohen, R. C. (2019). Direct observation of changing NOx lifetime in North American cities. *Science*, *366*(6466), 723–727. https://doi.org/10.1126/science.aax6832

Laughner, J. L., Zare, A., & Cohen, R. C. (2016). Effects of daily meteorology on the interpretation of space-based remote sensing of NO2. *Atmospheric Chemistry and Physics*, *16*(23), 15247–15264. https://doi.org/10.5194/acp-16-15247-2016

Laughner, J. L., Zhu, Q., & Cohen, R. C. (2019). Evaluation of version 3.0B of the BEHR OMI NO2 product. *Atmospheric Measurement Techniques*, *12*(1), 129–146. https://doi.org/10.5194/amt-12-129-2019

Lin, J. T., Liu, M. Y., Xin, J. Y., Boersma, K. F., Spurr, R., Martin, R. V., & Zhang, Q. (2015).

Influence of aerosols and surface reflectance on satellite NO2 retrieval: Seasonal and spatial characteristics and implications for NOx emission constraints. *Atmospheric Chemistry and Physics*, *15*(19), 11217–11241. https://doi.org/10.5194/acp-15-11217-2015

Liu, F., Page, A., Strode, S. A., Yoshida, Y., Choi, S., Zheng, B., et al. (2020). Abrupt declines in tropospheric nitrogen dioxide over China after the outbreak of COVID-19. Retrieved from http://arxiv.org/abs/2004.06542

Liu, M., Lin, J., Boersma, K. F., Pinardi, G., Wang, Y., Chimot, J., et al. (2019). Improved aerosol correction for OMI tropospheric NO2 retrieval over East Asia: constraint from CALIOP aerosol vertical profile. *Atmospheric Measurement Techniques*, *12*(1), 1–21. https://doi.org/10.5194/amt-12-1-2019

Lorente, A., Folkert Boersma, K., Yu, H., Dörner, S., Hilboll, A., Richter, A., et al. (2017). Structural uncertainty in air mass factor calculation for NO2 and HCHO satellite retrievals. *Atmospheric Measurement Techniques*, *10*(3), 759–782. https://doi.org/10.5194/amt-10-759-2017

McLinden, C. A., Fioletov, V. E., Boersma, K. F., Kharol, S. K., Krotkov, N., Lamsal, L. N., et al. (2014). Improved satellite retrievals of NO2 and SO2 over the Canadian oil sands and comparisons with surface measurements. *Atmospheric Chemistry and Physics*, *14*(7), 3637–3656. https://doi.org/10.5194/acp-14-3637-2014

McLinden, C. A., Fioletov, V. E., Krotkov, N. A., Li, C., Boersma, K. F., & Adams, C. (2016). A Decade of Change in NO2 and SO2 over the Canadian Oil Sands As Seen from Space. *Environmental Science and Technology*, *50*(1), 331–337. https://doi.org/10.1021/acs.est.5b04985

Moran, M. D., Ménard, S., Talbot, D., Huang, P., Makar, P. A., Gong, W., et al. (2009). *Particulate-Matter Forecasting with GEM-MACH15, A New Canadian Air-Quality Forecast Model. In Air Pollution Modeling and Its Application XX*. Retrieved from http://www.nato.int/science

NASA. (2020). Pandemic Before and After: Northeast US 2015-2019 versus 2020. Retrieved from https://airquality.gsfc.nasa.gov/slider/northeast-2020

Palmer, P. I., Jacob, D. J., Chance, K., Martin, R. V., Spurr, R. J. D., Kurosu, T. P., et al. (2001). Air mass factor formulation for spectroscopic measurements from satellites: Application to formaldehyde retrievals from the Global Ozone Monitoring Experiment. *Journal of Geophysical Research: Atmospheres*, *106*(D13), 14539–14550. https://doi.org/10.1029/2000JD900772

Pendlebury, D., Gravel, S., Moran, M. D., & Lupu, A. (2018). Impact of chemical lateral boundary conditions in a regional air quality forecast model on surface ozone predictions during stratospheric intrusions. *Atmospheric Environment*, *174*, 148–170. https://doi.org/10.1016/j.atmosenv.2017.10.052

Plumer, B., & Popovich, N. (2020). Traffic and Pollution Plummet as U.S. Cities Shut Down for Coronavirus. Retrieved from https://www.nytimes.com/interactive/2020/03/22/climate/coronavirus-usa-traffic.html

Pope, R. J., Chipperfield, M. P., Savage, N. H., Ordóñez, C., Neal, L. S., Lee, L. A., et al. (2015). Evaluation of a regional air quality model using satellite column NO2: Treatment of observation errors and model boundary conditions and emissions. *Atmospheric Chemistry and Physics*, *15*(10), 5611–5626. https://doi.org/10.5194/acp-15-5611-2015

Le Quéré, C., Jackson, R. B., Jones, M. W., Smith, A. J. P., Abernethy, S., Andrew, R. M., et al. (2020). Temporary reduction in daily global CO2 emissions during the COVID-19 forced confinement. *Nature Climate Change*, 1–7. https://doi.org/10.1038/s41558-020-0797-x

Reuter, M., Buchwitz, M., Schneising, O., Krautwurst, S., O'Dell, C. W., Richter, A., et al. (2019). Towards monitoring localized CO2 emissions from space: co-located regional CO2 and NO2 enhancements observed by the OCO-2 and S5P satellit. *Atmospheric Chemistry and Physics Discussions*, 1–19. https://doi.org/10.5194/acp-2019-15

Russell, A. R., Perring, A. E., Valin, L. C., Bucsela, E. J., Browne, E. C., Wooldridge, P. J., & Cohen, R. C. (2011). A high spatial resolution retrieval of NO2 column densities from OMI: Method and evaluation. *Atmospheric Chemistry and Physics*, *11*(16), 8543–8554. https://doi.org/10.5194/acp-11-8543-2011

Shah, V., Jacob, D. J., Li, K., Silvern, R. F., Zhai, S., Liu, M., et al. (2020). Effect of changing NOx lifetime on the seasonality and long-term trends of satellite-observed tropospheric NO2 columns over China. *Atmospheric Chemistry and Physics Discussions*, *20*(3), 1483–1495. https://doi.org/10.5194/acp-2019-670

Shen, L., & Mickley, L. J. (2017). Effects of El Niño on Summertime Ozone Air Quality in the Eastern United States. *Geophysical Research Letters*, *44*(24), 12,543-12,550. https://doi.org/10.1002/2017GL076150

Storrow, B. (2019). America’s mega-emitters are starting to close. Retrieved May 15, 2020, from https://www.eenews.net/stories/1060965553/

Valin, L. C., Russell, A. R., & Cohen, R. C. (2013). Variations of OH radical in an urban plume inferred from NO2 column measurements. *Geophysical Research Letters*, *40*(9), 1856–1860. https://doi.org/10.1002/grl.50267

VanDerA, R. J., Eskes, H. J., Boersma, K. F., van Noije, T. P. C., Van Roozendael, M., De Smedt, I., et al. (2008). Trends, seasonal variability and dominant NOx source derived from a ten year record of NO2 measured from space. *Journal of Geophysical Research Atmospheres*, *113*(4), 1–12. https://doi.org/10.1029/2007JD009021

VanGeffen, J. H. G. M., Eskes, H. J., Boersma, K. F., Maasakkers, J. D., & Veefkind, J. P. (2019). *TROPOMI ATBD of the total and tropospheric NO2 data products*. Retrieved from http://www.tropomi.eu/sites/default/files/files/publicS5P-KNMI-L2-0005-RP-ATBD_NO2_data_products-20190206_v140.pdf

Veefkind, J. P., Aben, I., McMullan, K., Förster, H., de Vries, J., Otter, G., et al. (2012). TROPOMI on the ESA Sentinel-5 Precursor: A GMES mission for global observations of the atmospheric composition for climate, air quality and ozone layer applications. *Remote Sensing of Environment*, *120*(2012), 70–83. https://doi.org/10.1016/j.rse.2011.09.027

Wang, C., Wang, T., & Wang, P. (2019). The Spatial–Temporal Variation of Tropospheric NO2 over China during 2005 to 2018. *Atmosphere*, *10*(8), 444. https://doi.org/10.3390/atmos10080444

Williams, J. E., Folkert Boersma, K., Le Sager, P., & Verstraeten, W. W. (2017). The high-resolution version of TM5-MP for optimized satellite retrievals: Description and validation. *Geoscientific Model Development*, *10*(2), 721–750. https://doi.org/10.5194/gmd-10-721-2017

Zhang, R., Zhang, Y., Lin, H., Feng, X., Fu, T.-M., & Wang, Y. (2020). NOx Emission Reduction and Recovery during COVID-19 in East China. *Atmosphere*, *11*(4), 433. https://doi.org/10.3390/atmos11040433

Zhao, X., Griffin, D., Fioletov, V., McLinden, C. A., Cede, A., Tiefengraber, M., et al. (2020). Assessment of the quality of TROPOMI high-spatial-resolution NO2 data products in the Greater Toronto Area. *Atmospheric Measurement Techniques*, *13*(4), 2131–2159. https://doi.org/10.5194/amt-13-2131-2020

Supporting Information for:

Disentangling the impact of the COVID-19 lockdowns on urban NO_2 from natural variability

Daniel L. Goldberg*[1,3], Susan C. Anenberg[1], Debora Griffin[2], Chris A. McLinden[2], Zifeng Lu[3], David G. Streets[3]

[1]Department of Environmental and Occupational Health, George Washington University, Washington, DC, U.S.
[2]Air Quality Research Division, Environment and Climate Change Canada (ECCC), Toronto, Ontario, Canada
[3]Energy Systems Division, Argonne National Laboratory, Lemont, IL, U.S.

*Corresponding author. Phone: (202)994-8102; Email: dgoldberg@gwu.edu

This PDF file includes:

Further description of TROPOMI NO_2 processing technique and associated uncertainties
Further description of methodologies using to calculate NO_2 drops during COVID-19
Figures S1 to S5
Table S1

1. TROPOMI NO_2

1.1 Air Mass Factors and Uncertainty Estimates

The slant tropospheric column is converted to a vertical column using a quantity known as the air mass factor (Palmer et al., 2001). The air mass factor is the most uncertain quantity in the retrieval algorithm (Lorente et al., 2017), and is a function of the surface reflectance, the NO_2 vertical profile, and scattering in the atmosphere among other factors (Lamsal et al., 2014). Using accurate and high-resolution data (spatially and temporally) as inputs in calculating the air mass factor can significantly reduce the overall errors of the air mass factor (Choi et al., 2019; Goldberg et al., 2017; Laughner et al., 2016, 2019; Lin et al., 2015; Liu et al., 2019; Russell et al., 2011; Zhao et al., 2020) and thus the tropospheric vertical column content.

Operationally, the TM5-MP model ($1 \times 1°$ resolution) (Williams et al., 2017) is used to provide the NO_2 vertical shape profile and the climatological Lambertian Equivalent Reflectivity ($0.5 \times 0.5°$ resolution) (Kleipool et al., 2008) is used to provide the surface reflectivities. The operational air mass factor calculation does not explicitly account for aerosol absorption effects, which are accounted for in the effective cloud radiance fraction. While the operational product does have larger uncertainties in the tropospheric column contents than a product with higher spatial resolution inputs, we limit our analysis to relative trends, which dramatically reduces this uncertainty. The uncertainty in any daily measurement in the operational slant column data has been assigned to be approximately 5.7×10^{14} molecules-cm^{-2} (van Geffen et al., 2020). This equates to roughly a 5-10% uncertainty over polluted areas. However, because we are averaging over many days (~20-40), we assume that random errors will cancel due to the large number of observations used. This leaves only the systematic errors. Here, we assign the AMFs and tropospheric vertical column contents a systematic uncertainty of 20% in the trends (McLinden et al., 2014). This systematic uncertainty may be largest over areas with changing snow cover, such as Minneapolis, Chicago, Toronto, and Montreal. We calculate total uncertainty as the quadrature of the uncertainty associated with this potential systematic bias and the standard deviation of the three Methods. These are listed in Table S1.

1.2 Re-gridding of TROPOMI NO_2

For our analysis we re-grid the operational TROPOMI tropospheric vertical column NO_2, with native pixels of approximately 3.5 × 7 km^2, to a newly defined 0.01° × 0.01° grid (approximately 1 × 1 km^2) centered over the continental United States (CONUS; corner points: SW: 24.5° N, 124.75° W; NE: 49.5° N, 66.75° W). Before re-gridding, the data are filtered so as to use only the highest quality measurements (quality assurance flag (QA_flag) > 0.75).

2. Description of Methodologies 2 & 3

2.1 Method 2: Normalization of Daily TROPOMI NO_2 using ERA5

We use TROPOMI NO_2 data from 2018 – 2019 as analog data to normalize 2020 data. Essentially, our method is searching through the 2018 – 2019 archive to find a meteorological analog to the current conditions and then adjusting the current day's conditions based off that analog.

For each day of the record, we modify the original observed TROPOMI NO_2 based on its value compared to a "baseline" which we set as a weekday in April with 3 m/s southwest winds. For each day, n, and each city, i, the normalized NO_2, $\widehat{NO_2}$, is calculated as follows:

$$\widehat{NO_2}_{n,i} = \frac{NO_{2_{n,i}}}{f_{total_{n,i}}}$$

The subscript i represents a city-specific average within a 0.4° × 0.4° box (i.e., ~20 km radius) surrounding the city center.

The four adjustment factors are: sun angle, wind speed, wind-direction, and day-of-week. While other conditions affect NO_2 amounts they are either interrelated to the aforementioned factors or can be considered secondary. Each of the four individual factors are multiplied together to get a "total adjustment factor". The "total adjustment factor", f_{total} is calculated for each day, n, and each city, i, as follows:

$$f_{total_{n,i}} = \left[f_{sun-angle}\right]_n \left[f_{day-of-week}\right]_n \left[f_{wind-speed}\right]_{n,i} \left[f_{wind-dir}\right]_{n,i}$$

For the sun angle factor, we calculate this using a cosine fit. For each julian date, *n*, the sun angle factor ($f_{sun\text{-}angle}$) can be calculated as follows:

$$f_{sun-angle_n} = \frac{0.75 + 0.25 * cos\left[2\pi \frac{n+11}{365}\right]}{0.75 + 0.25 * cos\left[2\pi \frac{n_d+11}{365}\right]}$$

At the winter solstice, December 21st (n = -11 or n = 354) the numerator value is 1 and at the summer solstice, June 21st (n = 171) the numerator value is 0.5. The variable n_d represents the normalization day, in this case April 15th (n_d = 105). The aforementioned equation is only valid for locations north of the Tropic of Cancer (23.4°N).

For the wind speed factor, we fit a third-order polynomial using analog winds speeds from the 2018 – 2019 TROPOMI time frame. Wind speeds of 5 m/s would yield a correction factor of 1. Values larger than 1 represent winds slower than 5 m/s and values smaller than 1 represent winds faster than 5 m/s. This fit allows us to calculate a correction factor given any city-specific wind speed.

For the wind direction factor, we calculate a correction factor normalized to southwest winds. Wind directions are grouped into the following categories: 0 – 90 º are southwest, 90 – 180 º are northwest, 180 – 270 º are northeast, and 270 – 360 º are southeast. Once the wind speed is grouped into a specific category, the factor is defined based on its relation to the climatological wind direction; northwest for New York City and Washington D.C., and northeast for Los Angeles. Daily winds which are typical of the climatological wind direction yield a correction factor of 1.

Lastly, for the day-of-week factor, we assume 15% lower values on Saturdays and 30% lower values on Sundays. We assume all weekdays have similar emissions rates to each other. Weekdays have a factor of 1, Saturdays a factor of 0.85 and Sundays a factor of 0.70. These assumptions are broadly consistent with literature demonstrating day-of-week NO_X emissions patterns.

As an example, a stagnant day in January may be lowered by a factor of ~2 to "normalize" to a 5 m/s April weekday, whereas a very windy weekend day in April might be increased by a factor of 1.5 to account for the faster than normal winds and the weekend effect.

Method 3: Normalization of Daily TROPOMI NO_2 using a CTM

We infer expected NO_2 columns (V_{ex}) during the lock-down period (t_{covid}) using the output from the GEM-MACH model(Moran et al., 2009; Pendlebury et al., 2018). The operational version of the model, used in this study, has a 10 × 10 km^2 grid cell size with 80 vertical levels (from the surface to about 0.1 hPa), provides hourly output, and includes emissions, chemistry, dispersion, and removal processes of 41 gaseous and eight particle species. The emissions used in the model are processed using the Sparse Matrix Operator Kernel Emissions (SMOKE)(Coats, n.d.) and account for seasonal changes; changes in emissions due to the COVID-10 lock-downs are not considered in the model framework.

In a first step the GEM-MACH NO_2 vertical levels in the boundary layer (up to approximately 2 km) are summed to a column amount using the model's pressure and temperature profile(Côté et al., 1998). Since the GEM-MACH model currently does not contain any NO_x sources in the free troposphere (such as aircraft or lightning emissions), the NO_2 model concentrations decrease to 0 above the planetary boundary layer (PBL). A free tropospheric column (from 2 km to 12 km) is added to the GEM-MACH PBL vertical column densities (VCDs) using a monthly GEOS-Chem run (0.5x0.67^0 resolution, version v8-03-01; http://www.geos-chem.org)(Bey et al., 2001; McLinden et al., 2014). The model VCDs are then mapped in space and time to the TROPOMI observations, and treated like the observations, where data with qa<0.75 are filtered and averaged over the city center using a 28-day running mean.

The expected VCDs (V_{ex}) are the 28-day running means of the modelled VCDs (V_M) during the lockdown period (t_{covid}). V_{ex} is scaled to remove any bias between the model and satellite (V_T) for the pre-lockdown period (t_{pre}, between February 1st and March 1st 2020):

$$V_{ex}(t_{covid}) = V_M(t_{covid}) \cdot mean\left(\frac{V_T(t_{pre})}{V_M(t_{pre})}\right).$$

Depending on the city, some dates within the t_{pre} time period may not be considered for the scaling, if there is a strong divergence between the model and the observations.

The estimated NO_2 drop is the average of the difference between the expected VCDs, $V_{ex}(t_{covid})$, and the observed TROPOMI VCDs, $V_T(t_{covid})$, between March 28th and April 16th, 2020 using the daily 28-day running means as shown in Figure 4.

3. Supplemental Figures

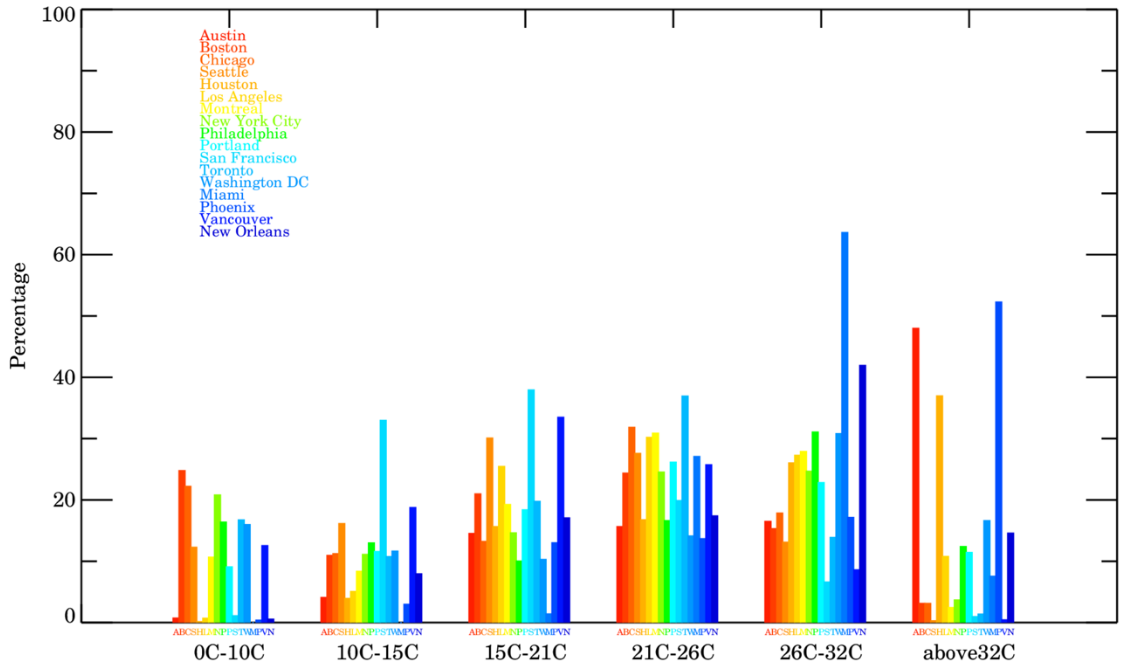

Figure S1. Frequency of daily maximum 2-m temperature within each bin, according to the ERA5 re-analysis. Each bar is a different city as noted by list in top left.

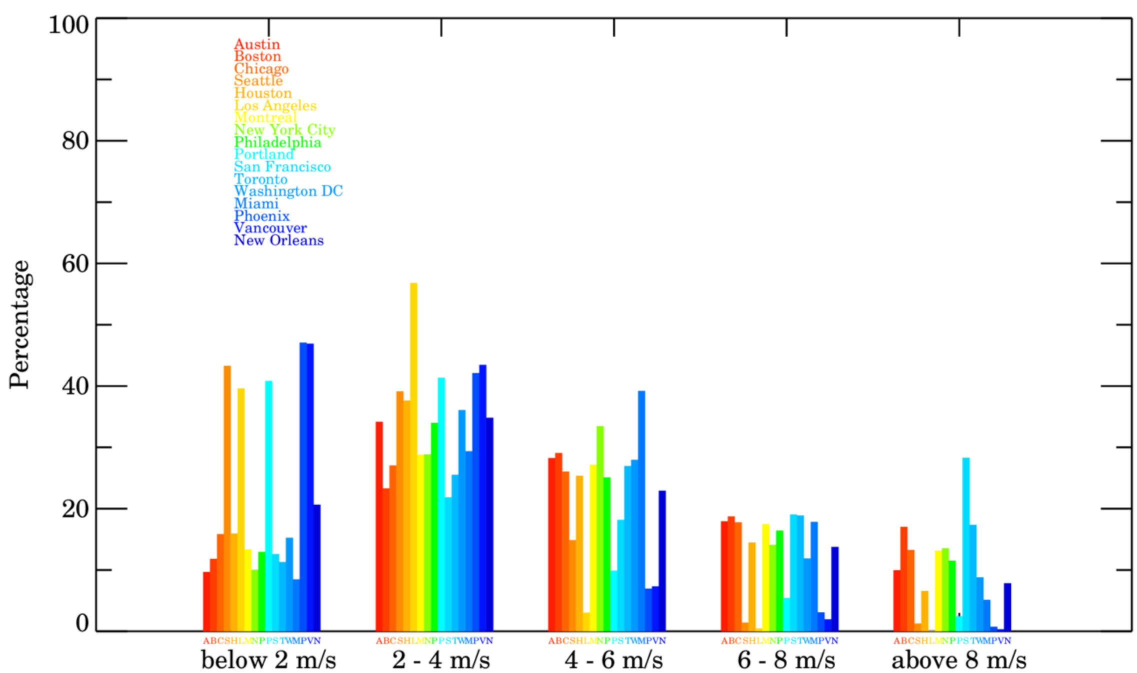

Figure S2. Frequency of 100-m afternoon (16Z-21Z) wind speed within each bin, according to the ERA5 re-analysis. Each bar is a different city as noted by list in top left.

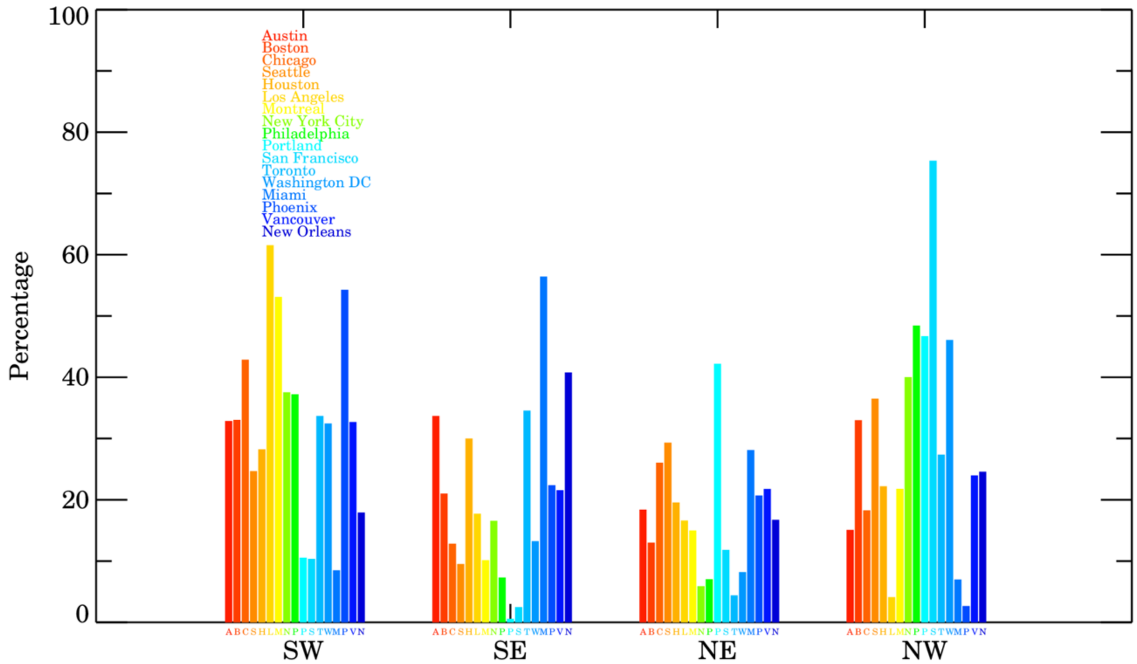

Figure S3. Frequency of 100-m afternoon (16Z-21Z) wind direction within each bin, according to the ERA5 re-analysis. Each bar is a different city as noted by list in top left.

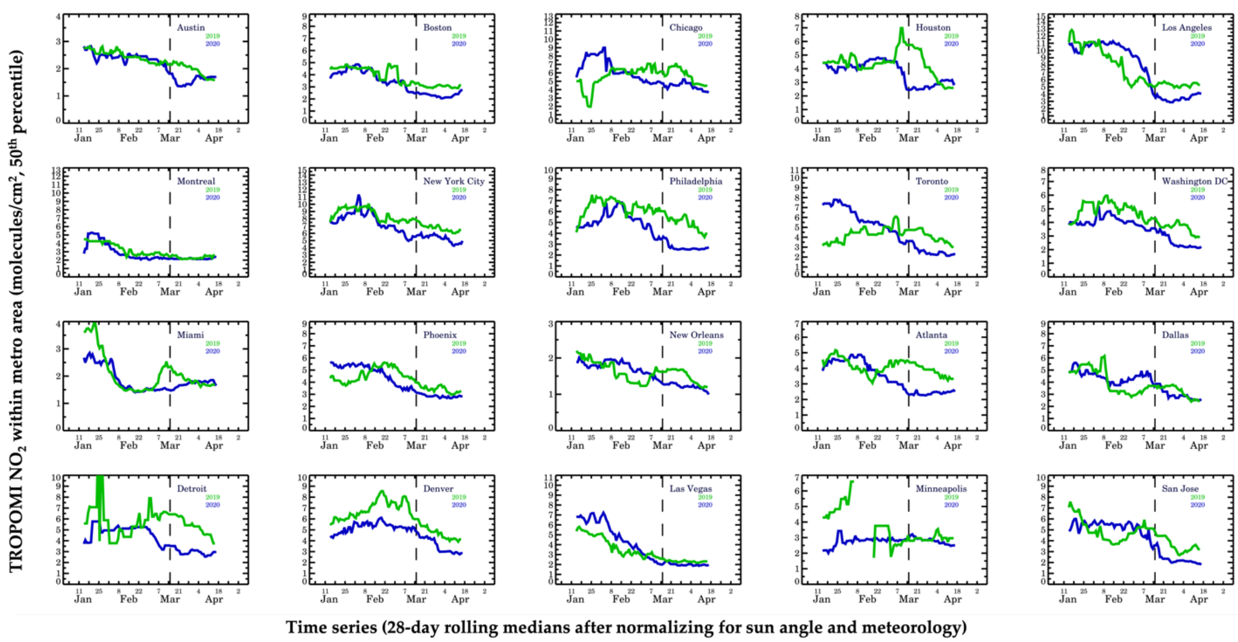

Figure S4. Trends in TROPOMI NO_2 since January 1 in 2019 and 2020. The lines represent the 28-day rolling median value (50th percentile) in a 0.4° × 0.4° box centered on the city center for the largest cities (New York City, Los Angeles, Chicago, Toronto, Houston) and 0.2° × 0.2° box in all other cities.

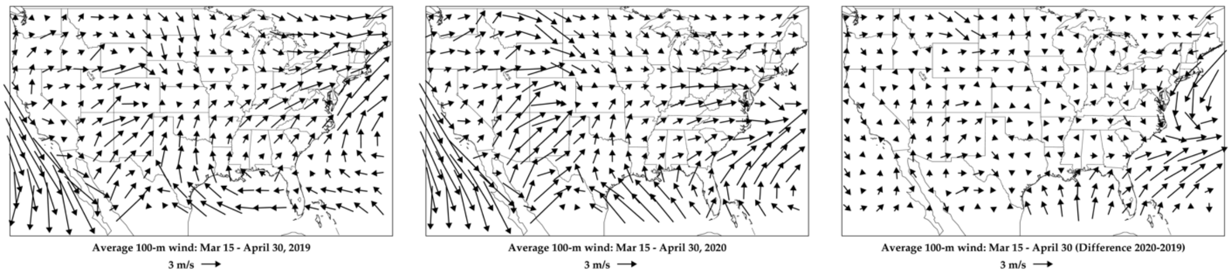

Figure S5. Average 100-m afternoon (16Z-21Z) wind speed and direction for March 15 – April 30 in (left) 2019, (center) 2020, (right) difference between the two years, according to the ERA5 re-analysis.

4. Supplemental Table

Table S1. Uncertainties associated with our methodology. Uncertainties are calculated as the quadrature of any potential systematic bias (20%) and the standard deviation of Methods 1 – 3.

City Name	Uncertainty
San Jose	20.1%
Toronto	20.3%
Los Angeles	23.6%
Philadelphia	21.3%
Atlanta	21.5%
Detroit	21.4%
Denver	21.2%
Montreal	20.2%
Boston	23.5%
Washington DC	24.2%
New York City	20.0%
New Orleans	20.5%
Las Vegas	26.1%
Phoenix	23.4%
Chicago	22.4%
Houston	23.6%
Austin	20.3%
Dallas	21.1%
Miami	22.0%
Minneapolis	20.3%

References

Bey, I., Jacob, D. J., Yantosca, R. M., Logan, J. A., Field, B. D., Fiore, A. M., et al. (2001). Global modeling of tropospheric chemistry with assimilated meteorology: Model description and evaluation. *Journal of Geophysical Research: Atmospheres*, *106*(D19), 23073–23095. https://doi.org/10.1029/2001JD000807

Choi, S., Lamsal, L. N., Follette-Cook, M., Joiner, J., Krotkov, N. A., Swartz, W. H., et al. (2019). Assessment of NO2 observations during DISCOVER-AQ and KORUS-AQ field campaigns. *AMTD*. https://doi.org/10.5194/amt-2019-338

Coats, C. J. (n.d.). *High-performance algorithms in the Sparse Matrix Operator Kernel Emissions (SMOKE) Modeling System, American Meteorological Society, Atlanta, GA. USA, proceedings of the Ninth AMS Joint Conference on Applications of Air Pollution Meteorology with AWMA.*

Côté, J., Gravel, S., Méthot, A., Patoine, A., Roch, M., Staniforth, A., et al. (1998). The Operational CMC–MRB Global Environmental Multiscale (GEM) Model. Part I: Design Considerations and Formulation. *Http://Dx.Doi.Org/10.1175/1520-0493(1998)126<1373:TOCMGE>2.0.CO;2*. https://doi.org/10.1175/1520-0493(1998)126<1373:TOCMGE>2.0.CO;2

van Geffen, J., Boersma, K. F., Eskes, H., Sneep, M., ter Linden, M., Zara, M., & Veefkind, J. P. (2020). S5P TROPOMI NO₂ slant column retrieval: method, stability, uncertainties and comparisons with OMI. *Atmospheric Measurement Techniques*, *13*(3), 1315–1335. https://doi.org/10.5194/amt-13-1315-2020

Goldberg, D. L., Lamsal, L. N., Loughner, C. P., Swartz, W. H., Lu, Z., & Streets, D. G. (2017). A high-resolution and observationally constrained OMI NO2 satellite retrieval. *Atmospheric Chemistry and Physics*, *17*(18), 11403–11421. https://doi.org/10.5194/acp-17-11403-2017

Kleipool, Q. L., Dobber, M. R., de Haan, J. F., & Levelt, P. F. (2008). Earth surface reflectance climatology from 3 years of OMI data. *Journal of Geophysical Research Atmospheres*, *113*(18), 1–22. https://doi.org/10.1029/2008JD010290

Lamsal, L. N., Krotkov, N. A., Celarier, E. A., Swartz, W. H., Pickering, K. E., Bucsela, E. J., et al. (2014). Evaluation of OMI operational standard NO2 column retrievals using in situ and surface-based NO2 observations. *Atmospheric Chemistry and Physics*, *14*(21), 11587–11609. https://doi.org/10.5194/acp-14-11587-2014

Laughner, J. L., Zare, A., & Cohen, R. C. (2016). Effects of daily meteorology on the interpretation of space-based remote sensing of NO2. *Atmospheric Chemistry and Physics*, *16*(23), 15247–15264. https://doi.org/10.5194/acp-16-15247-2016

Laughner, J. L., Zhu, Q., & Cohen, R. C. (2019). Evaluation of version 3.0B of the BEHR OMI NO2 product. *Atmospheric Measurement Techniques*, *12*(1), 129–146. https://doi.org/10.5194/amt-12-129-2019

Lin, J. T., Liu, M. Y., Xin, J. Y., Boersma, K. F., Spurr, R., Martin, R. V., & Zhang, Q. (2015). Influence of aerosols and surface reflectance on satellite NO2 retrieval: Seasonal and spatial characteristics and implications for NOx emission constraints. *Atmospheric Chemistry and Physics*, *15*(19), 11217–11241. https://doi.org/10.5194/acp-15-11217-2015

Liu, M., Lin, J., Boersma, K. F., Pinardi, G., Wang, Y., Chimot, J., et al. (2019). Improved aerosol correction for OMI tropospheric NO2 retrieval over East Asia: constraint from CALIOP aerosol vertical profile. *Atmospheric Measurement Techniques*, *12*(1), 1–21. https://doi.org/10.5194/amt-12-1-2019

Lorente, A., Folkert Boersma, K., Yu, H., Dörner, S., Hilboll, A., Richter, A., et al. (2017). Structural uncertainty in air mass factor calculation for NO2 and HCHO satellite retrievals. *Atmospheric Measurement Techniques*, *10*(3), 759–782. https://doi.org/10.5194/amt-10-759-2017

McLinden, C. A., Fioletov, V. E., Boersma, K. F., Kharol, S. K., Krotkov, N., Lamsal, L. N., et al. (2014). Improved satellite retrievals of NO2 and SO2 over the Canadian oil sands and comparisons with surface measurements. *Atmospheric Chemistry and Physics*, *14*(7), 3637–3656. https://doi.org/10.5194/acp-14-3637-2014

Moran, M. D., Ménard, S., Talbot, D., Huang, P., Makar, P. A., Gong, W., et al. (2009). *Particulate-Matter Forecasting with GEM-MACH15, A New Canadian Air-Quality Forecast Model. In Air Pollution Modeling and Its Application XX*. Retrieved from http://www.nato.int/science

Palmer, P. I., Jacob, D. J., Chance, K., Martin, R. V., Spurr, R. J. D., Kurosu, T. P., et al. (2001). Air mass factor formulation for spectroscopic measurements from satellites: Application to formaldehyde retrievals from the Global Ozone Monitoring Experiment. *Journal of Geophysical Research: Atmospheres*, *106*(D13), 14539–14550. https://doi.org/10.1029/2000JD900772

Pendlebury, D., Gravel, S., Moran, M. D., & Lupu, A. (2018). Impact of chemical lateral boundary conditions in a regional air quality forecast model on surface ozone predictions during stratospheric intrusions. *Atmospheric Environment*, *174*, 148–170. https://doi.org/10.1016/j.atmosenv.2017.10.052

Russell, A. R., Perring, A. E., Valin, L. C., Bucsela, E. J., Browne, E. C., Wooldridge, P. J., & Cohen, R. C. (2011). A high spatial resolution retrieval of NO2 column densities from OMI: Method and evaluation. *Atmospheric Chemistry and Physics*, *11*(16), 8543–8554. https://doi.org/10.5194/acp-11-8543-2011

Williams, J. E., Folkert Boersma, K., Le Sager, P., & Verstraeten, W. W. (2017). The high-resolution version of TM5-MP for optimized satellite retrievals: Description and validation. *Geoscientific Model Development*, *10*(2), 721–750. https://doi.org/10.5194/gmd-10-721-2017

Zhao, X., Griffin, D., Fioletov, V., McLinden, C. A., Cede, A., Tiefengraber, M., et al. (2020). Assessment of the quality of TROPOMI high-spatial-resolution NO2 data products in the Greater Toronto Area. *Atmospheric Measurement Techniques*, *13*(4), 2131–2159. https://doi.org/10.5194/amt-13-2131-2020